Calibration of Sn-119 isomer shift using ab initio wave function methods

Kurian, Reshmi; Filatov, Michael

Published in:
Journal of Chemical Physics

DOI:
10.1063/1.3094259

Publication date:
2009

Calibration of ^{119}Sn isomer shift using *ab initio* wave function methods

Reshmi Kurian and Michael Filatov[a)]
Theoretical Chemistry, Zernike Institute for Advanced Materials, Rijksuniversiteit Groningen, Nijenborgh 4, 9747 AG Groningen, The Netherlands

(Received 23 December 2008; accepted 10 February 2009; published online 31 March 2009)

The isomer shift for the 23.87 keV M1 resonant transition in the ^{119}Sn nucleus is calibrated with the help of *ab initio* calculations. The calibration constant $\alpha(^{119}\mathrm{Sn})$ obtained from Hartree–Fock (HF) calculations ($\alpha_{\mathrm{HF}}(^{119}\mathrm{Sn})=(0.081\pm0.002)a_0^{-3}$ mm/s) and from second-order Møller–Plesset (MP2) calculations ($\alpha_{\mathrm{MP2}}(^{119}\mathrm{Sn})=(0.091\pm0.002)a_0^{-3}$ mm/s) are in good agreement with the previously obtained values. The importance of a proper treatment of electron correlation effects is demonstrated on the basis of a statistical analysis of the results of the calibration. The approach used in the calibration is applied to study the ^{119}Sn isomer shift in $CaSnO_3$ perovskite under pressure. Comparison with the experimental results for the pressure range of 0–36 GPa shows that the current methodology is capable of describing tiny variations of isomer shift with reasonable accuracy. © *2009 American Institute of Physics*. [DOI: 10.1063/1.3094259]

I. INTRODUCTION

Mössbauer or nuclear γ-resonance spectroscopy[1] is a widely used method for the investigation of the electronic structure of crystalline and disordered materials. An important advantage of Mössbauer spectroscopy is that it is capable of providing information about the local chemical environment of the resonating nuclei on an atomic scale.[2–9] The dependence of the energy of the nuclear γ-transition E_γ on the interaction with the surrounding electrons is at the heart of the method and provides its high sensitivity to the electronic structure of the sample. The isomer shift of a Mössbauer spectrum is a sensitive characteristic of the local chemical environment of the resonating nucleus, which provides information on the charge and spin state of the target atom and on the geometry of its coordination sphere. The isomer shift is defined as a displacement of the frequency of the nuclear γ-transition in the target (absorber) nucleus ΔE_γ^a with respect to the reference (source) nucleus ΔE_γ^s as given in Eq. (1) in terms of the Doppler velocity necessary to achieve resonance.

$$\delta=\frac{c}{E_\gamma}(\Delta E_\gamma^a-\Delta E_\gamma^s). \tag{1}$$

Traditionally, the energy differences $\Delta E_\gamma^{a(s)}$ are calculated within the framework of perturbation theory, whereby the variation of the electron-nuclear interaction potential during the γ-transition is treated as a weak perturbation of the nuclear energy levels.[10–14] This approach leads to the well known expression for the isomer shift of Mössbauer spectra as a linear function of the so-called contact electron density (electron density at the nucleus) in the target $\bar{\rho}_e^a$ and reference $\bar{\rho}_e^s$ compounds, see Eq. (2).

$$\delta=\alpha(\bar{\rho}_e^a-\bar{\rho}_e^s). \tag{2}$$

The calibration constant α, in Eq. (2), depends entirely on fundamental constants and on the internal parameters of the nuclear γ-transition. Although these parameters, the most important of which are the nuclear charge radius R and the variation of the nuclear charge radius ΔR in the γ-transition, and the contact density $\bar{\rho}_e^{a(s)}$ are physical observables, modern experimental techniques do not allow for a sufficiently accurate determination of these quantities. The theoretical calculation of the electron contact density at the target nuclei in chemical compounds remains the most reliable way of determining of the calibration constant α.

It should be realized, however, that the success of the traditional approach based on Eq. (2) relies on the availability of the contact densities from theoretical calculations. The contact density is easily available from calculations in which the theoretical methods fulfilling the Hellmann–Feynman theorem, such as the self-consistent field (SCF) method or the Kohn–Sham method of density functional theory (DFT), are employed.[15–17] However, the use of the most sophisticated methods of *ab initio* wave function theory, such as the coupled-cluster method or single-reference and multireference Møller–Plesset perturbation theory, requires the calculation of the so-called relaxed density matrix[18] which considerably increases the amount of computational work necessary to obtain the density. Hence relatively low-level computational methods are commonly employed in the calibration of the Mössbauer isomer shift using Eq. (2). Furthermore, as a consequence of the approximations embedded into Eq. (2) when deriving it from Eq. (1), the inclusion of relativistic effects into the calculated contact densities is not a straightforward task.[14,19] Relativity strongly modifies electronic wave functions in the vicinity of the nuclei, such that its inclusion is mandatory for obtaining accurate results for properties depending on the atomic core electrons.[14,20]

In this respect, the situation in theoretical modeling of the Mössbauer isomer shift is dramatically different from the modeling of another important parameter of the Mössbauer

a)Author to whom correspondence should be addressed. Electronic mail: m.filatov@rug.nl.

spectrum, the quadrupole splitting, for theoretical determination of which the most sophisticated computational methods including the coupled-cluster method with relativistic corrections can be employed. Note that the quadrupole splitting parameters are obtained within the finite-difference scheme which does not rely on the availability of the fully relaxed density matrix.[21,22] It is desirable therefore to employ, for the calibration of the Mössbauer isomer shift, a more direct theoretical approach which allows for straightforward inclusion of the most important effects, such as relativity and electron correlation. Such an approach, which is based on the nonperturbative inclusion of the finite size nucleus into theoretical calculations, has been recently developed in Refs. 23 and 24. Within this approach, the isomer shifts are calculated based on the numeric differentiation of the electronic energy with respect to the nuclear radius and hence it overcomes the need of the computation of relaxed density matrix in higher order Møller–Plesset or coupled-cluster methods.[23,24] This offers possibility for a systematic improvement of the results of theoretical modeling of the Mössbauer isomer shift.

In the present work, the new method is applied to the calibration of the Mössbauer isomer shift of ^{119}Sn nucleus. Tin compounds have been extensively studied with the use of Mössbauer spectroscopy and there exists a plethora of experimental data on the ^{119}Sn isomer shift in various chemical environments.[25–27] Accurate theoretical simulations of the experimental data over a wide range of chemical environments are used to obtain a theoretical value of the calibration constant α, which is compared to the previously obtained values. In this work, special emphasis is given to the use of systematically improvable *ab initio* wave function methods and on the role of the electron correlation effects for obtaining accurate theoretical results. As an independent test of the calibration constant $\alpha(^{119}\mathrm{Sn})$ obtained, theoretical simulations of the pressure dependence of the Mössbauer isomer shift in $CaSnO_3$ perovskite are carried out. It is our hope that the calibration of the ^{119}Sn isomer shift on a representative set of compounds carried out with the use of accurate computational methods will help improve the accuracy of interpretation of the experimental measurements.

II. THEORY AND COMPUTATIONAL DETAILS

The isomer shift is calculated using the new approach,[23] according to which the isomer shift is expressed as a derivative of the electronic energy with respect to the radius of a finite size nucleus. This method has the advantage that the effects of relativity and electron correlation can be straightforwardly incorporated into the theoretical isomer shifts. The isomer shift is expressed as

$$\delta = \frac{c}{E_\gamma}\left(\left.\frac{\delta E_e^a(R)}{\delta R}\right|_{R=R_N} - \left.\frac{\delta E_e^s(R)}{\delta R}\right|_{R=R_N}\right)\Delta R, \tag{3}$$

where E_γ is the energy of the nuclear γ-transition, c is the velocity of light, R is the nuclear radius, ΔR is the variation of the nuclear radius from the experimental value R_N, and E_e^a and E_e^s are the electronic energies of systems containing the absorber and the source nuclei. The derivatives $(\delta E_e^a(R)/\delta R)$ and $\delta E_e^s(R)/\delta R$ are calculated numerically using the increment of 10^{-6} bohr for the root mean square nuclear charge radius[28] ($R_{\mathrm{Sn}}=0.876\,94\times10^{-4}$ bohr). Throughout this work, the Gaussian nucleus model[28] is used in the calculations.

In analogy to the conventional approach based on Eq. (2), the effective electron density inside the nucleus $\bar{\rho}_e$ can be defined as in Eq. (4),[23]

$$\bar{\rho}_e = \frac{5}{4\pi ZR}\left.\frac{\delta E_e^a(R)}{\delta R}\right|_{R=R_N}. \tag{4}$$

The contact density obtained in this way can be used in connection with Eq. (2). Thus, the calibration constant α in Eq. (2) can be obtained from a linear regression as given in Eq. (5) (Refs. 15–17) where the effective contact densities [Eq. (4)] are employed

$$\delta = \alpha\bar{\rho} + b. \tag{5}$$

Equation (5) is used to calculate the isomer shifts from the contact densities using the calibration parameters, α and b specific for each method of calculation.

All calculations were carried out using the COLOGNE 2005 (Ref. 29) suite of programs in which the computational scheme for the isomer shift calculation is implemented. The relativistic calculations are carried out within the one-electron approximation[30] and using the normalized elimination of the small component method.[31]

The calculations were carried out both at the Hartree–Fock (HF) and second-order Møller–Plesset perturbation theory[32] (MP2) level. The spin-unrestricted formalism was applied for open-shell species. The $21s15p11d2f$ basis set of Dyall[33] was used for Sn and for all other elements the augmented correlation consistent double-zeta (aug-cc-pVDZ) basis sets of Dunning[34] were used. All basis sets were used in uncontracted form.

The Sn compounds used in the present investigation are SnF_4, SnO_2, $CaSnO_3$, $BaSnO_3$, $SnCl_4$, SnS_2, $SnBr_4$, $SnSe_2$, SnI_4, SnO, SnS, SnSe, and $SnCl_2$. The isomer shift of these compounds ranges from -0.36 mm/s (SnF_4) to $+4.06$ mm/s ($SnCl_2$) (see Table II). The sources of the experimental values for each of these compounds are cited in Table II. In this work, we employed the embedded cluster approach to calculate the local electronic structure of solids. Within this approach, a cluster of atoms representing a structural unit of the crystalline solid is immersed in the Madelung potential of the rest of the crystal. The Madelung potential is modeled by a large array of point charges placed at the appropriate crystallographic positions. The magnitudes of the charges are determined from the natural bond order analysis[35] of the respective cluster wave functions calculated at the HF level. From our preliminary calculations we concluded that the inclusion of the Madelung potential of the crystal has a relatively minor effect on the calculated contact densities [Eq. (4)], which is consistent with the conclusions of other works.[15,16] However, because the clusters modeling the above solids are negatively charged, the embedding potential was added to compensate for the extra negative cluster charge.

The crystal structures and the cluster geometries considered in the present work are explained below. The cluster

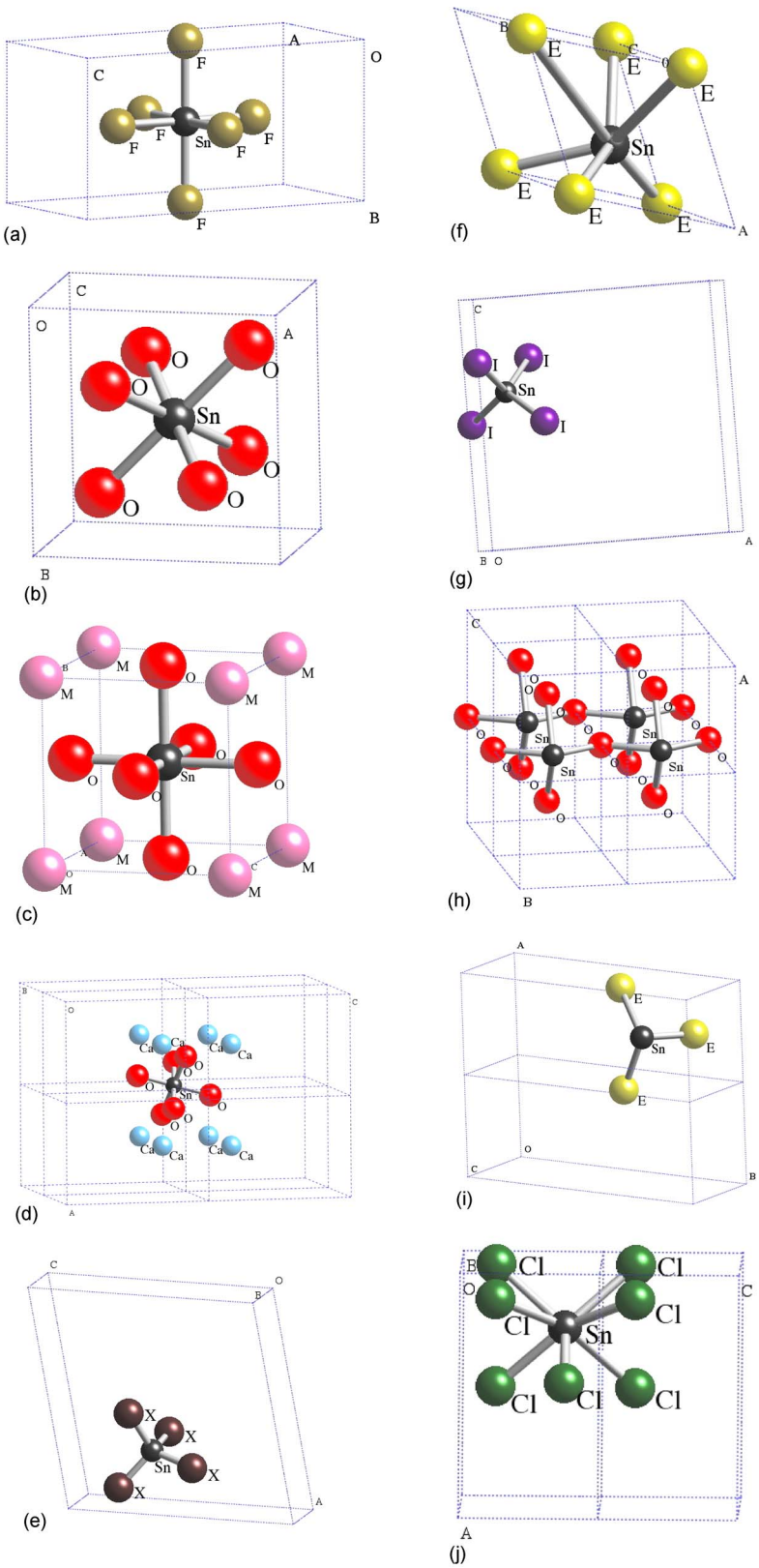

FIG. 1. (Color online) The cluster geometries used in the calculations, (a) $[SnF_6]^{2-}$ in SnF_4 (b) $[SnO_6]^{8-}$ in SnO_2 (c) $[SnO_6]^{8-}\cdot 8M^{2+}$, M=Ca/Ba in $CaSnO_3$/$BaSnO_3$, respectively (d) $[SnO_6]^{8-}\cdot 8Ca^{2+}$ in $CaSnO_3$ perovskite (e) $[SnX_4]$, X=Cl/Br in $SnCl_4$/$SnBr_4$, respectively (f) $[SnE_6]^{8-}$, E=S/Se in SnS_2/$SnSe_2$, respectively (g) $[SnI_4]$ in SnI_4 (h) $[Sn_4O_{14}]^{20-}$ in SnO (i) $[SnE_3]^{4-}$, E=S/Se in SnS/SnSe, respectively (j) $[SnCl_7]^{5-}$ in $SnCl_2$.

geometries are shown in Fig. 1. The coordinates of atoms in the clusters and of point charges used to simulate the Madelung potential were obtained from the crystal structures using the VICS II (Ref. 36) program.

SnF_4 (Ref. 37) has a body-centered-tetragonal structure. The cluster is $[SnF_6]^{2-}$, where the tin atom is surrounded by a distorted octahedron of fluorine atoms [see Fig. 1(a)]. The atomic positions are in the $14/mmm$ space group.

SnO_2 (Ref. 38) has a rutile, tetragonal structure ($P4_2/mnm$). The cluster on which calculations were done is $[SnO_6]^{8-}$, where the tin atom is surrounded by a distorted octahedron of oxygen atoms [see Fig. 1(b)].

$CaSnO_3$ and $BaSnO_3$ (Ref. 39) have cubic structures ($Pm\bar{3}m$). The tin atoms are in a cubic environment where the Ca/Ba ions lie in the cube vertices and O atoms lie in the middle of all cube edges. The cluster considered is $[SnO_6]^{8-}$, with the eight Ca^{2+}/Ba^{2+} ions around the cluster modeled by the respective Stuttgart effective core potentials[40] (ECPs) [see Fig. 1(c)].

$CaSnO_3$, considered in the Sec. III B, has an orthorhombically distorted perovskite structure[41] ($Pnma$). It consists of corner-linked SnO_6 octahedra with the Ca ions in the ninefold oxygen coordination. The cluster considered is $[SnO_6]^{8-}$ with eight Ca^{2+} ions around the cluster (which is modeled by Stuttgart ECPs). The tin atom is in an environment of oxygen octahedron [see Fig. 1(d)].

$SnCl_4$ (Ref. 56) and $SnBr_4$ (Ref. 43) have monoclinic structures ($P2_1/c$) with four molecules per unit cell. The molecular clusters $SnCl_4$ and $SnBr_4$, with distorted tetrahedral geometry, were considered for the calculations [see Fig. 1(e)].

SnS_2 and $SnSe_2$ (Ref. 48) have a layered structure ($P\bar{3}m1$). The sulfide or selenide anions form a hexagonal close-packed arrangement while the tin cations fill alternating layers of octahedral sites. The crystal consists of *X-M-X* sandwiches (where *M* is Sn and *X* is S in SnS_2 and Se in $SnSe_2$). The unit cell contains two molecules. The clusters are $[SnS_6]^{8-}$ and $[SnSe_6]^{8-}$, where the coordination around the Sn atom is that of a distorted octahedron [see Fig. 1(f)].

SnI_4 (Ref. 44) has a cubic lattice ($Pa\bar{3}$) with eight molecules packing loosely in the unit cell. The cluster considered is SnI_4 with a distorted tetrahedral geometry [see Fig. 1(g)].

SnO (Ref. 45) has a tetragonal structure ($P4/nmm$) with four tin atoms in the unit cell. The chemically meaningful structural unit of this crystal includes four closely packed SnO_4 tetragonal pyramidal blocks pairwise connected via bridged oxygen atoms. For this crystal, we included all four tin atoms in the unit cell into the representative cluster, which resulted in a $[Sn_4O_{14}]^{20-}$ cluster embedded in the Madelung field of the rest of the crystal [see Fig. 1(h)].

SnS and SnSe (Ref. 46) have an orthorhombic structure ($Pnma$). The clusters considered for these solids are $[SnS_3]^{4-}$ and $[SnSe_3]^{4-}$ in which the tin atom has three pyramidal S/Se neighbors, two located in the plane of the layer and one at a short distance normal to this plane [see Fig. 1(i)].

$SnCl_2$ (Ref. 47) has an orthorhombic structure ($Pnam$) with four $SnCl_2$ units per unit cell. All atoms in the unit cell lie in two planes parallel to (001). The cluster is $[SnCl_7]^{5-}$, in which the tin atom is surrounded with three chlorine atoms at distances of 2.68, 3.21, and 3.30 Å in the same plane, two chlorine atoms at distances of 2.78 Å and two chlorine atoms at a distance of 3.05 Å [see Fig. 1(j)].

III. RESULTS AND DISCUSSION

In this section, we present the results of the theoretical determination of the ^{119}Sn calibration constant α which is obtained from the linear relationship [Eq. (5)] between the theoretically calculated contact densities with the experimental isomer shifts in a series of tin compounds. The calibration parameters obtained from the linear regression analysis will be used to calculate the ^{119}Sn isomer shifts, which will be compared to the available experimental values. As an independent test of the quality of the obtained calibration parameters, a calculation of the isomer shift in $CaSnO_3$ perovskite under pressure will be undertaken.

TABLE I. Electron contact densities of ^{119}Sn clusters (a large constant of 182 800a_0^{-3} has been subtracted from all the values) along with structural references.

	Space group	Ref.	SCF	MP2
SnF_4	$14/mmm$	37	13.32	23.84
SnO_2	$P4_2/mnm$	38	17.50	29.68
$CaSnO_3$	$Pm\bar{3}m$	39	15.25	27.92
$BaSnO_3$	$Pm\bar{3}m$	39	16.46	26.51
$SnCl_4$	$P2_1/c$	56	27.50	35.19
SnS_2	$P\bar{3}m1$	48	27.37	40.60
$SnBr_4$	$P21/c$	43	30.94	40.39
$SnSe_2$	$P\bar{3}m1$	48	30.37	43.66
SnI_4	$Pa\bar{3}$	44	35.28	45.17
SnO	$P4/nmm$	45	44.00	55.50
SnS	$Pnma$	46	57.03	64.23
SnSe	$Pnma$	46	58.65	65.28
$SnCl_2$	$Pnam$	47	67.43	72.14

A. Calibration of the ^{119}Sn isomer shift

The electron contact densities calculated using Eq. (4) are reported in Table I along with the experimental ^{119}Sn isomer shifts. The results of linear regression analysis of the theoretical contact densities versus the experimental isomer shifts are presented in Fig. 2. Besides the contact densities obtained in the present work with the use of the relativistically corrected HF and MP2 methods, the contact densities obtained by Svane *et al.*[27] as an average of the total electronic densities obtained in periodic density functional calculations with the local density approximation (LDA) functional inside a sphere of nuclear charge radius, are also used in the linear regression analysis and are reported in Fig. 2.

The calibration parameters obtained from the linear regression in Fig. 2 are $\alpha_{HF}(^{119}\text{Sn})=(0.081\pm0.002)a_0^{-3}$ mm/s, $b_{HF}=(-14\,807.91\pm467.11)$ mm/s and $\alpha_{MP2}(^{119}\text{Sn})=(0.091\pm0.002)a_0^{-3}$ mm/s, $b_{MP2}=(-16\,584.65\pm378.40)$ mm/s, respectively. The α_{MP2} value is in good agreement with the calibration constant $\alpha_{LDA}(^{119}\text{Sn})=(0.092\pm0.002)a_0^{-3}$ mm/s, obtained from the periodic LDA calculations.[27] Given that both methods, MP2 and LDA, include electron correlation, good agreement between the results of different sets of calculations indicates the importance of inclusion of correlation effects into the isomer shift calculations. The results of the statistical analysis of the data reported in Table I and in Fig. 2 support this conclusion. The MP2 method shows a much lower standard deviation in the linear regression analysis and an improved r^2 correlation coefficient as compared to the HF values, $\sigma_{MP2}=0.114$ mm/s versus $\sigma_{HF}=0.158$ mm/s and $r^2_{MP2}=0.994$ versus $r^2_{HF}=0.989$.

It is noteworthy that a systematic improvement of the results of the theoretical calculations can be achieved with

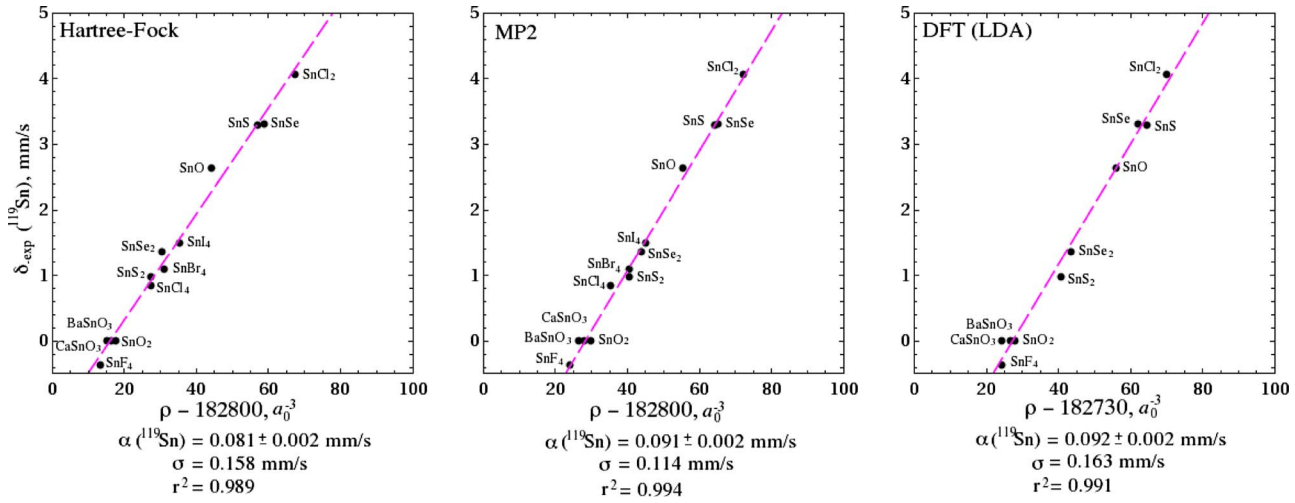

FIG. 2. (Color online) Calculated electron contact density (in a_0^{-3}) vs experimental isomer shifts (in mm/s) for Sn clusters using SCF, MP2, and DFT (LDA) (Ref. 27), respectively.

the use of the methods which take electron correlation into account. Indeed, electron correlation results in a noticeable contraction of the electron density towards the nucleus, which is evident from the contact densities reported in Table I and from literature data.[49] Besides that, the inclusion of electron correlation results in an improved description of the bond covalency in metal complexes, which plays an important role for a reliable determination of the contact densities as has been demonstrated by Sadoc *et al.*[50] In this respect, it is rather surprising that the LDA periodic calculations[27] yield a somewhat inferior statistical correlation with the experimental data than the MP2 embedded cluster calculation, $\sigma_{MP2}=0.114$ mm/s versus $\sigma_{LDA}=0.163$ mm/s. This suggests that with the use of wave function based methods one achieves a more efficient system-specific account of the important electron correlation effects. Although the comparison has been made against the LDA calculations, judging from the results of density functional calculations of Mössbauer isomer shifts[16,17,24] the use of the gradient-corrected functionals should not lead to a marked improvement of the correlation with experiment. The use of the hybrid functionals, however, may lead to an improved correlation with experiment and may bring the accuracy of density functional calculations closer to the wave function methods.[16,17,24]

The calibration parameters $\alpha(^{119}\text{Sn})$ and $b(^{119}\text{Sn})$ obtained with the HF and MP2 methods were used to calculate the ^{119}Sn isomer shifts using Eq. (5). The resulting ^{119}Sn isomer shifts are compared in Table II with the experimental values and with the values obtained from the calibration parameters and contact densities reported in Ref. 27. The re-

TABLE II. Experimental isomer shifts and isomer shifts calculated according to Eq. (5) using the contact densities given in Table I and the calibration constants obtained from linear fits in Fig. 2.

	δ_{expt}	Ref.	SCF	MP2	LDA[a]
SnF_4	−0.36	54	−0.23	−0.37	−0.28
SnO_2	0.00	55	0.03	−0.01	0.07
$CaSnO_3$	0.00	55	0.11	−0.13	−0.28
$BaSnO_3$	0.00	55	−0.07	0.15	−0.06
$SnCl_4$	0.85	56	0.92	0.65	n.a.
SnS_2	0.98	42	0.91	1.15	1.23
$SnBr_4$	1.13	59	1.20	1.13	n.a.
$SnSe_2$	1.36	57 and 58	1.15	1.42	1.48
SnI_4	1.55	59	1.55	1.56	n.a.
SnO	2.64	60	2.26	2.50	2.63
SnS	3.29	42 and 61–63	3.31	3.29	3.43
SnSe	3.31	61 and 57	3.44	3.38	3.21
$SnCl_2$	4.06	64	4.50	4.01	3.94
MAE[b]			0.13	0.08	0.12
σ[c]			0.15	0.11	0.16
MSE[d]			0.02	0.01	0.01

[a]Calculated using the densities and calibration constants obtained from the periodic LDA calculations in Ref. 27.
[b]Mean absolute error of the method.
[c]Standard deviation of the points.
[d]Mean signed error of the method.

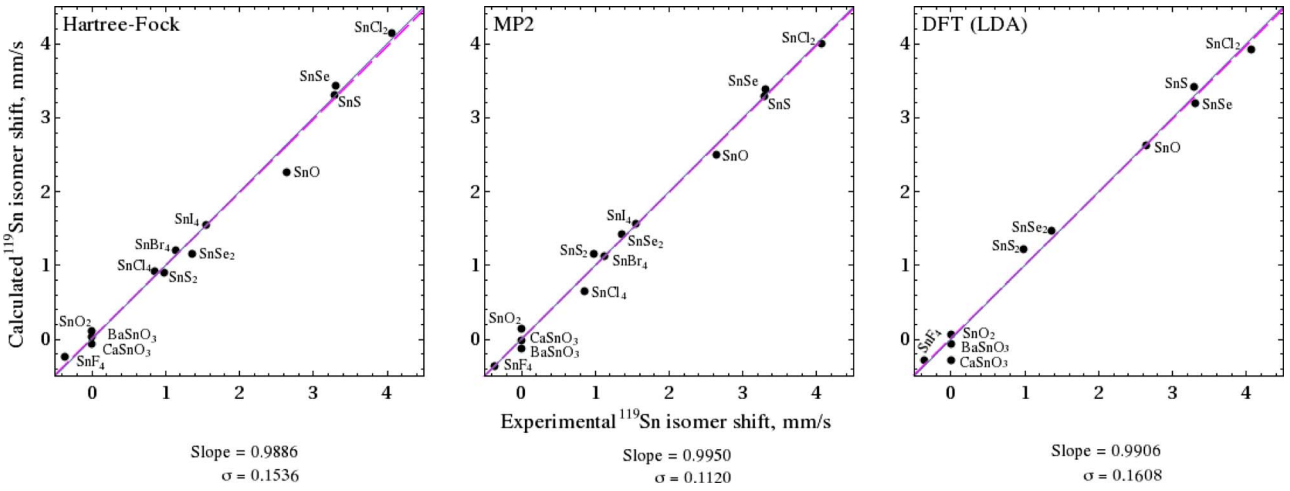

FIG. 3. (Color online) Calculated isomer shifts (in mm/s) vs experimental isomer shifts (in mm/s) for Sn clusters using SCF, MP2, and DFT (LDA) (Ref. 27), respectively.

sults of the linear regression analysis of the theoretical isomer shifts versus the experimental values are presented in Fig. 3. Again, the MP2 method provides an improved statistical correlation of the theoretical isomer shift values with experiment. It is gratifying that the MP2 method provides a better statistical correlation with experiment than the earlier reported periodic LDA calculations of Svane *et al.*,[27] $\sigma_{MP2}=0.112$ mm/s versus $\sigma_{LDA}=0.160$ mm/s. The average errors in the calculations also strengthen this argument, $MAE_{MP2}=0.08$ mm/s versus $MAE_{LDA}=0.12$ mm/s (refer Table II). Taken together with an improvement in the calibration procedure brought about by the inclusion of electron correlation in the MP2 method, this observation provides strong evidence of the importance of proper description of electron correlation effects in the calculation of isomer shifts in metal compounds.

B. Isomer shift variation in $CaSnO_3$ perovskite

The calibration constants obtained in Sec. III A were employed to calculate the variation of ^{119}Sn isomer shift in $CaSnO_3$ perovskite. Recently, experimental results for the dependence of the isomer shift under external pressure have been obtained in Ref. 51. The range of variation of the isomer shift is −0.08 mm/s for the pressure range of 0–36 GPa. No phase transitions have been observed in $CaSnO_3$ perovskite under high pressure so that the isomer shift variation is entirely due to the change in the local geometry around the tin sites.[51]

For a theoretical method employed for the calculation of isomer shifts, the variation of the isomer shift of $CaSnO_3$ perovskite under pressure represents a stringent test. Indeed, the range of isomer shifts in this case is rather narrow, much narrower than the range in the different compounds used in Sec. III A. Therefore, the ability of a theoretical method to reproduce these variations with a reasonable accuracy should indicate the quality of the computational approach. In the previous work,[51] a value of +0.008 mm/s was obtained at a pressure of 36 GPa by using traditional approach based on the MO-LCAO (molecular orbital as a linear combination of the atomic orbitals) calculations.[52] Besides being an order of magnitude too small, this value has the wrong sign which indicates certain inconsistencies in the theoretical method employed in Ref. 51.

In the present work, we employed the unit cell parameters of $CaSnO_3$ perovskite determined in Ref. 53 for the pressure range from 0 to 8.5 GPa. The fractional coordinates of atoms in the unit cell were taken from Ref. 41 at 0 GPa pressure. Because the information on the fractional atomic coordinates of $CaSnO_3$ perovskite under nonzero pressure is not available from literature, these coordinates were kept fixed in the calculations. The lattice parameters for pressures greater than 8.5 GPa were obtained by an extrapolation of the parameters obtained experimentally for the 0–8.5 GPa pressure range. Although the lack of accurate information on the fractional coordinates and the lattice parameters may lead to certain errors in the calculations, we adopted this approach in the present work following Ref. 51, where the unit cell parameters were obtained in a similar way.

The dependence of the ^{119}Sn isomer shift in $CaSnO_3$ perovskite calculated with the use of the HF and MP2 methods is plotted in Fig. 4 along with the experimental curve.[51] For each theoretical method, the calibration constants α and

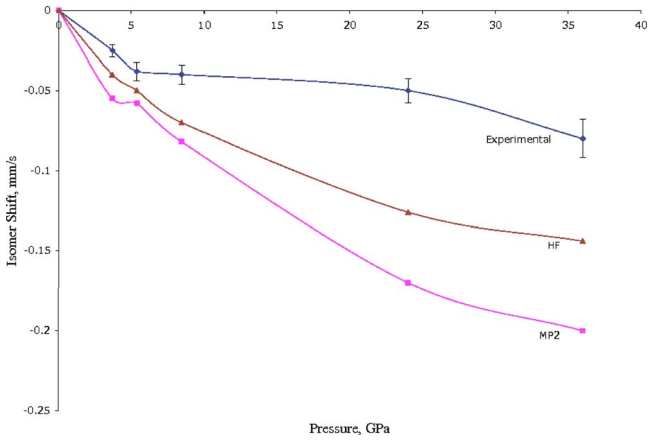

FIG. 4. (Color online) Pressure variation (in GPa) vs isomer shift (in mm/s) for $CaSnO_3$ perovskite structure. Experimental values are taken from Ref. 51.

b [see Eq. (5)] obtained in Sec. III A are employed. The maximum variations of the ^{119}Sn isomer shift obtained with the use of the HF and MP2 method are −0.14 and −0.20 mm/s, respectively. Note that the theoretical isomer shift variations have the same sign as the experimentally measured ones and that the theoretically obtained curves in Fig. 4 follow the profile of the experimental curve.[51]

The discrepancy between the calculated and the experimental variations of the isomer shift most likely can be attributed to the inaccuracies in the determination of the geometry of the clusters used in the present calculations. Note that with the use of similarly obtained local geometries a much lower value of +0.008 mm/s of the isomer shift variation at 36 GPa was obtained in Ref. 51. It is also noteworthy that, in the pressure range of 0–8.5 GPa, where at least the experimental lattice parameters are available, the discrepancy between the calculated and experimental isomer shifts is rather small. The second-order Doppler shift (SODS) due to the lattice vibration represents yet another factor which can influence the results of the isomer shift measurements under high pressure.[65] The omission of this contribution in the calibration of the isomer shift does not affect the quality of calibration because all experimental data have been obtained under the ambient pressure. Although the SODS makes a negligibly small contribution at the ambient pressure[65] it may affect the relative isomer shifts calculated with respect to the ambient pressure, such as those reported in Fig. 4. Therefore, the comparison with the experiment is incomplete and does not allow one to draw a clear conclusion on the superior performance of one of the methods. Nevertheless, the results reported in Fig. 4 give us confidence that the present theoretical scheme is capable of providing qualitative estimates of tiny variations of the isomer shift due to pressure. Because, in the presence of phase transitions, the isomer shift variation is typically much greater[66,67] than that found in Ref. 51, we expect that the present theoretical method should enable one to describe the variations of isomer shift in phase transitions with sufficient confidence.

IV. CONCLUSION

Reliable theoretical determination of the hyperfine parameters of Mössbauer active nuclei still remains one of the challenging tasks in computational chemistry. The interpretation of Mössbauer isomer shifts necessitates the determination of a method-independent value of the calibration constant α, which connects the electron density in the vicinity of the nucleus and the isomer shift via Eq. (2).

In the present work, we have undertaken a theoretical study of the calibration constant α of the ^{119}Sn nucleus using recently developed methodology which is based on a definition of the isomer shift as a derivative of the total electronic energy with respect to the nuclear charge radius.[23] Tin is one of the best studied Mössbauer nuclei and the availability of a large amount of data facilitates a reliable calibration. In a number of previous studies, calibration constants $\alpha(^{119}\mathrm{Sn})$ ranging from $0.17a_0^{-3}$ mm/s (Ref. 68) to $0.037a_0^{-3}$ mm/s (Ref. 69) have been obtained from the experimental and theoretical data. The most recent theoretical value of the $\alpha(^{119}\mathrm{Sn})$ constant is $(0.092\pm0.002)a_0^{-3}$ mm/s as obtained in the periodic density functional calculations of Svane *et al.*[27] The calibration constant $\alpha_{\mathrm{MP2}}(^{119}\mathrm{Sn})=(0.091\pm0.002)a_0^{-3}$ mm/s obtained in the present work with the use of relativistically corrected MP2 calculations is in excellent agreement with the previously obtained value. This gives us confidence that a method-independent value of the calibration constant can indeed be determined in theoretical calculations.

One of the interesting observations made in the course of the present work is the importance of including electron correlation in the theoretical modeling of the Mössbauer isomer shift. Indeed, as shown in the linear regression analysis of the calculated contact densities [see Eq. (4)] with respect to the observed isomer shifts, the use of the MP2 method leads to a noticeable improvement of the statistical correlation as compared to the HF results (see Fig. 2). Besides that, the description of the isomer shifts calculated with the correlated method (MP2) are in a much better agreement with the experimental values than the HF results (see Table II and Fig. 3). This finding implies that a systematic improvement in modeling of Mössbauer parameters can be achieved with the use of systematically improvable *ab initio* methods. It is expected that even better agreement with the experiment can be achieved with the use of more sophisticated methods of quantum chemistry, such as the coupled-cluster method [CCSD(T)] or the multireference second-order perturbation theory method (CASPT2).

An independent verification of the quality of the ^{119}Sn calibration constants obtained in this work is achieved in the calculation of variation of the ^{119}Sn isomer shift in $CaSnO_3$ perovskite under pressure. Reasonable agreement of the theoretical values of the isomer shift in the pressure range of 0–36 GPa with the experimental values has been reached. However, more precise information on the variation of the lattice parameters and atomic fractional coordinates is necessary to provide a more reliable description of isomer shifts. Nevertheless, the ability of the computational approach employed in the present work to correctly describe very tiny variations of the isomer shift resulting from the change in local geometry under pressure is encouraging. It is our hope that with the use of the current theoretical approach one can achieve a reliable interpretation of the experimental Mössbauer spectra in situations where simple models based on intuitive arguments may fail.

[1] R. L. Mössbauer, Z. Phys. **151**, 124 (1958).
[2] O. Leupold, J. Pollmann, E. Gerdau, H. D. Rüter, G. Faigel, M. Tegze, G. Bortel, R. Rüffer, A. I. Chumakov, and A. Q. R. Baron, Europhys. Lett. **35**, 671 (1996).
[3] I. Koyama, Y. Yoda, X. W. Zhang, M. Ando, and S. Kikuta, Jpn. J. Appl. Phys., Part 1 **35**, 6297 (1996).
[4] R. Coussement, S. Cottenier, and C. L'abbé, Phys. Rev. B **54**, 16003 (1996).
[5] G. Neyens, J. Odeurs, R. Coussement, C. L'abbé, S. Cottenier, and J. Ladriére, Hyperfine Interact. **111**, 341 (1998).
[6] O. Leupold, A. I. Chumakov, E. E. Alp, W. Sturhahn, and A. Q. R. Baron, Hyperfine Interact. **123–124**, 611 (1999).
[7] C. L'abbé, R. Callens, and J. Odeurs, Hyperfine Interact. **135**, 275 (2001).
[8] A. Konjhodzic, A. Adamczyk, F. Vagizov, Z. Hasan, E. E. Alp, W. Sturhahn, J. Zhao J. J. Carroll, Hyperfine Interact. **170**, 83 (2006).
[9] D. A. Shirley and H. Haas, Annu. Rev. Phys. Chem. **23**, 385 (1972).
[10] G. K. Wertheim, *Mossbauer Effect: Principles and Applications* (Aca-

demic, New York, 1964).
[11] *Mössbauer Isomer Shifts*, edited by G. K. Shenoy and F. E. Wagner (North-Holland, Amsterdam, 1978).
[12] P. Gütlich, R. Link, and A. Trautwein, *Mössbauer Spectroscopy and Transition Metal Chemistry* (Springer, Heidelberg, 1978).
[13] L. R. Walker, G. K. Wertheim, and V. Jaccarino, Phys. Rev. Lett. **6**, 98 (1961).
[14] D. A. Shirley, Rev. Mod. Phys. **36**, 339 (1964).
[15] W. C. Nieuwpoort, D. Post, and P. T. van Duijnen, Phys. Rev. B **17**, 91 (1978).
[16] F. Neese, Inorg. Chim. Acta **337**, 181 (2002).
[17] V. N. Nemykin and R. G. Hadt, Inorg. Chem. **45**, 8297 (2006).
[18] J. Gauss and D. Cremer, Adv. Quantum Chem. **23**, 205 (1992).
[19] J. L. K. F. de Vries, J. M. Trooster, and P. Ros, J. Chem. Phys. **63**, 5256 (1975).
[20] G. Breit, Phys. Rev. **42**, 348 (1932).
[21] M. Pernpointner and L. Visscher, J. Chem. Phys. **114**, 10389 (2001).
[22] C. R. Jacob, L. Visscher, C. Thierfelder, and P. Schwerdtfeger, J. Chem. Phys. **127**, 204303 (2007).
[23] M. Filatov, J. Chem. Phys. **127**, 084101 (2007).
[24] R. Kurian and M. Filatov, J. Chem. Theory Comput. **4**, 278 (2008).
[25] J. Terra and D. Guenzburger, Hyperfine Interact. **60**, 627 (1990); Phys. Rev. B **44**, 8584 (1991); J. Phys.: Condens. Matter **3**, 6763 (1991).
[26] K. Jackson, S. Srinivas, J. Kortus, and M. Pederson, Phys. Rev. B **65**, 214201 (2002).
[27] A. Svane, N. E. Christensen, C. O. Rodrigues, and M. Methfessel, Phys. Rev. B **55**, 12572 (1997).
[28] L. Visscher and K. G. Dyall, At. Data Nucl. Data Tables **67**, 207 (1997); O. Visser, P. J. C. Aerts, D. Hegarty, and W. C. Niewpoort, Chem. Phys. Lett. **134**, 34 (1987).
[29] E. Kraka, J. Gräfenstein, M. Filatov, V. Polo, A. Wu, Y. He, L. Olsson, Z. Konkoli, Z. He, J.. Gauss, F. Reichel, and D. Cremer, COLOGNE 2005, Göteborg University, Göteborg, 2005.
[30] K. G. Dyall, J. Chem. Phys. **115**, 9136 (2001); J. Comput. Chem. **23**, 786 (2002).
[31] K. G. Dyall, J. Chem. Phys. **106**, 9618 (1997); M. Filatov and K. G. Dyall, Theor. Chem. Acc. **117**, 333 (2007).
[32] C. Møller and M. S. Plesset, Phys. Rev. **46**, 618 (1934); for a recent review, see D. Cremer, in *Encyclopedia of Computational Chemistry*, edited by P. v. R. Schleyer, N. L. Allinger, T. Clark, J. Gasteiger, P. A. Kollman, H. F. Schaefer III, and P. R. Schreiner (Wiley, Chichester, 1998), Vol. 3, p. 1706.
[33] K. G. Dyall, Theor. Chem. Acc. **99**, 366 (1998); **115**, 441 (2006).
[34] T. H. Dunning, J. Chem. Phys. **90**, 1007 (1989).
[35] J. E. Carpenter and F. Weinhold, J. Mol. Struct.: THEOCHEM **169**, 41 (1988); J. P. Foster and F. Weinhold, J. Am. Chem. Soc. **102**, 7211 (1980); A. E. Reed and F. Weinhold, J. Chem. Phys. **78**, 4066 (1983); A. E. Reed, R. B. Weinstock, and F. Weinhold, *ibid.* **83**, 735 (1985).
[36] F. Izumi and R. A. Dilanian, IUCR Newsl. **32**, 59 (2005).
[37] R. Hoppe and W. Dähne, Naturwiss. **49**, 254 (1962).
[38] W. H. Baur, Acta Crystallogr. **9**, 515 (1956).
[39] H. D. Megaw, Proc. Phys. Soc. London **58**, 133 (1946).
[40] P. Fuentealba, L. von Szentpaly, H. Preuss, and H. Stoll, J. Phys. B **18**, 1287 (1985).
[41] A. Vegas, M. Vallet-Regí, J. M. González-Calbet, snd M. A. Alario-Franco, Acta Crystallogr. Sect. B: Struct. Science **42**, 167 (1986).
[42] J. Grothaus and P. Boolchand, J. Non-Cryst. Solids **72**, 1 (1985).
[43] P. Brand and H. Sackmann, Acta Crystallogr. **16**, 446 (1963).
[44] F. Meller and I. Frankuchen, Acta Crystallogr. **8**, 343 (1955).
[45] F. Izumi, J. Solid State Chem. **38**, 381 (1981).
[46] H. Wiedemeir and H. G. von Schnering, Z. Kristallogr. **148**, 295 (1978).
[47] J. M. van den Berg, Acta Crystallogr. **14**, 1002 (1961).
[48] R. W. G. Wyckoff, *Crystal Structures* (Wiley, New York, 1964).
[49] C. F. Fischer and J. S. Carley, J. Phys. B **9**, 29 (1976).
[50] A. Sadoc, R. Broer, and C. de Graaf, Chem. Phys. Lett. **454**, 196 (2008).
[51] G. N. Stepanov, Phys. Solid State **48**, 1284 (2006).
[52] P. E. Lippens, Phys. Rev. B **60**, 4576 (1999).
[53] J. Kung, R. J. Angel, and N. L. Ross, Phys. Chem. Miner. **28**, 35 (2001).
[54] L. Fournès, J. Grannec, Y. Potin, and P. Hagenmuller, Solid State Commun. **59**, 833 (1986).
[55] J. G. Stevens, Hyperfine Interact. **13**, 221 (1983).
[56] N. W. G. Debye and M. Linzer, J. Chem. Phys. **61**, 4770 (1974).
[57] P. Boolchand, J. Grothaus, W. J. Bresser, and P. Suranyi, Phys. Rev. B **25**, 2975 (1982).
[58] R. H. Herber, A. E. Smelkinson, M. J. Sienko, and L. F. Schneemeyer, J. Chem. Phys. **68**, 3705 (1978).
[59] J. G. Stevens and M. A. Groforth, ^{119}Sn *Mössbauer Spectroscopy* (Mössbauer Effect Data Center, Asheville, NC, 1993).
[60] R. H. Herber, Phys. Rev. B **27**, 4013 (1983).
[61] V. Fano and I. Ortalli, J. Chem. Phys. **61**, 5017 (1974).
[62] J. K. Lees and P. A. Flinn, J. Chem. Phys. **48**, 882 (1968).
[63] J. C. Jumas, S. del Bucchia, E. Phillippot, and M. Maurin, J. Solid State Chem. **41**, 50 (1982).
[64] S. R. A. Bird, J. D. Donaldson, and J. Silver, J. Chem. Soc. Dalton Trans. **1972**, 1950.
[65] U. D. Wdowik and K. Ruebenbauer, Phys. Rev. B **76**, 155118 (2007).
[66] P. A. Magill and L. D. Roberts, Phys. Rev. B **37**, 399 (1988).
[67] R. D. Taylor, M. Pasternak, and J. N. Farrell, Hyperfine Interact. **40**, 351 (1988).
[68] J. P. Bocquet, Y. Y. Chu, O. C. Kistner, M. L. Perlman, and G. T. Emery, Phys. Rev. Lett. **17**, 809 (1966).
[69] K. Mazheika, D. Baltrunas, A. Dragunas, K. Makariunas, and V. Remeikis, Lith. Phys. J. **38**, 7 (1998).